

Evolution of Phonon Transport Across Structural Phase Transitions in MgAgSb

Luman Shang

*Advanced Thermal Management Technology and Functional Materials Laboratory,
Ministry of Education Key Laboratory of NSLSCS, School of Energy and Mechanical Engineering,
Nanjing Normal University, Nanjing 210023, P. R. China*

Yu Wu*

*Advanced Thermal Management Technology and Functional Materials Laboratory,
Ministry of Education Key Laboratory of NSLSCS, School of Energy and Mechanical Engineering,
Nanjing Normal University, Nanjing 210023, P. R. China*

Yufan Liu

*Advanced Thermal Management Technology and Functional Materials Laboratory,
Ministry of Education Key Laboratory of NSLSCS, School of Energy and Mechanical Engineering,
Nanjing Normal University, Nanjing 210023, P. R. China*

Shuming Zeng

College of Physics Science and Technology, Yangzhou University, Jiangsu, Yangzhou 225009, China

Gang Tang

School of Interdisciplinary Science, Beijing Institute of Technology, Beijing 100081, China

Chenhan Liu†

*Advanced Thermal Management Technology and Functional Materials Laboratory,
Ministry of Education Key Laboratory of NSLSCS, School of Energy and Mechanical Engineering,
Nanjing Normal University, Nanjing 210023, P. R. China*

MgAgSb, a promising thermoelectric material, undergoes reversible phase transitions that drastically alter its thermal transport behavior. Using first-principles calculations, we systematically investigate the lattice thermal conductivity (κ_L) of its three phases: α , β , and γ , revealing a progressive increase following $\alpha < \beta < \gamma$. This trend originates from distinct scattering mechanisms. Four-phonon scattering substantially suppresses the particle-like conductivity (κ_p) in the β and γ phases, while electron-phonon scattering provides a minor additional reduction. In contrast, the wave-like conductivity (κ_c) from coherent phonon tunneling is highest in the complex α phase, contributing up to 44% of κ_L . Notably, the temperature dependence of κ_L differs fundamentally between phases: in β , the weak κ_p variation arises from a decreasing Grüneisen parameter with temperature; in α , the strong rise in κ_c with temperature counteracts the decay of κ_p . Our findings establish a comprehensive picture of thermal transport in MgAgSb, highlighting the phase-dependent interplay between particle-like and wave-like phonon contributions.

I. INTRODUCTION

Understanding lattice thermal transport across structural phase transitions is important for both fundamental phonon physics and the optimization of thermoelectric (TE) materials[1–5]. In crystalline solids, heat conduction is commonly described within the Peierls–Boltzmann framework, where phonons are treated as particle-like quasiparticles characterized by well-defined group velocities and lifetimes[6–8]. This description works well for simple crystals with weakly overlapping phonon branches, but it can become insufficient in structurally complex materials, strongly anharmonic systems, and compounds with dense low-lying optical modes.

In such cases, heat transport may also involve couplings between different vibrational eigenstates, giving rise to a coherent contribution beyond the conventional phonon-gas picture[9–12]. The unified Wigner formulation provides a natural framework for this regime by decomposing the lattice thermal conductivity (κ_L) into a particle-like term (κ_p) and a wave-like coherent term (κ_c)[13–15], thereby connecting the Peierls limit of simple crystals with the Allen–Feldman-like regime of complex and glasslike solids. In recent years, this framework has proved especially useful for materials with ultralow or weakly temperature-dependent thermal conductivity (κ)[16–19].

At present, accurate first-principles predictions for thermal transport increasingly require going beyond the traditional three phonon (3ph) approximation. When lower-order channels are limited or anharmonicity is strong, four phonon (4ph) scattering has been proven

* wuyu@njnu.edu.cn

† chenhanliu@njnu.edu.cn

to produce significant corrections[20–22]. A reliable description of the phase-dependent κ requires simultaneously addressing higher-order anharmonic scattering[23–25] and coherent off-diagonal transport[15, 26]. This has been confirmed in the study of the multiphase CsPbBr₃, where considering 4ph instead of only 3ph results in a 40% reduction in κ_L [27]. Meanwhile, in metallic or semimetallic systems, electron-phonon (el-ph) scattering can become another decay pathway for the phonons that thermal transport[28–31]. For example, in TaN, after considering el-ph scattering, the κ_L decreases by 15.6%[32, 33].

MgAgSb is an excellent material to address this question[34–37]. As a near-room-temperature TE material, α -MgAgSb exhibits favorable electrical transport together with intrinsically low κ_L , which has been associated with its distorted crystal structure, weak hierarchical bonding, and suppression of transverse acoustic phonons[38–41]. MgAgSb also undergoes successive structural transitions from the low-temperature α phase to the intermediate β phase and then to the high-temperature γ phase, accompanied by substantial changes in symmetry, disorder, and electronic structure. In particular, the α phase is semiconducting[36]. And theoretical calculations of the β and γ phases in their stable structures show that they are metallic[42], implying that el-ph scattering may become relevant in these phases. Although previous studies have clarified the crystal structures and TE properties of individual MgAgSb phases, and have identified microscopic origins of the ultralow κ in α -MgAgSb, a unified picture of heat transport across the α - β - γ sequence is still lacking, especially with respect to the interplay among κ_p , κ_c , 4ph scattering, and el-ph scattering.

In this work, we systematically investigate the κ_L of α -, β -, and γ -MgAgSb from first principles within a unified thermal-transport framework. By combining the κ_p and the κ_c , and by explicitly incorporating 3ph, 4ph, and el-ph scattering where appropriate, we establish a comprehensive microscopic picture of phase-dependent heat transport in this system. We show that 4ph scattering strongly suppresses κ_p in the β and γ phases, while el-ph scattering provides an additional reduction. By contrast, the coherent contribution is most significant in the structurally complex α phase, where it accounts for a remarkably large fraction of κ_L . We further show that the temperature dependence of κ_L differs qualitatively among the three phases: the weak variation of κ_p in the β phase is linked to a reduction in the Grüneisen parameter with increasing temperature, whereas in the α phase the growth of κ_c partly compensates the decay of κ_p , leading to an unusually weak overall temperature dependence. These results clarify the microscopic origin of thermal transport across phase transitions in MgAgSb and highlight the need to treat particle-like transport, coherent vibrational coupling, higher-order anharmonicity, and el-ph scattering on an equal footing in phase-change TE materials.

II.COMPUTATIONAL METHODS

First-principles calculations were performed using the Vienna Ab Initio Simulation Package (VASP) based on density functional theory (DFT)[43], employing the projector augmented-wave (PAW) method with the PBEsol exchange-correlation functional[44]. A plane-wave cutoff energy of 520 eV was used. Atomic positions are optimized with an energy convergence criterion of 10^{-8} eV between consecutive steps and a maximum Hellmann-Feynman force tolerance of 10^{-6} eV/Å. The primitive cells of the α (24 atoms), β (6 atoms), and γ (3 atoms) phases were optimized using Γ -centered \mathbf{q} -meshes of $5 \times 5 \times 5$, $8 \times 8 \times 5$, and $9 \times 9 \times 9$, respectively.

For the *ab initio* molecular dynamics (AIMD) simulations, supercells containing 192 atoms were constructed for each phase by expanding their respective optimized primitive cells: $2 \times 2 \times 2$ supercell for the α phase, $4 \times 4 \times 2$ supercell for the β phase, and $4 \times 4 \times 4$ supercell for the γ phase. The AIMD simulations were run for 20 ps with a 1 fs timestep, employing a Γ -centered $1 \times 1 \times 1$ \mathbf{k} -mesh. The temperature-dependent effective potential (TDEP)[45, 46] method was then used to extract the second-, third-, and fourth-order interatomic force constants (IFCs). The cutoff radii for the second-, third-, and fourth-order IFCs were set to 10, 6, and 3 Å for the α phase, 10, 6, and 4 Å for the β phase, and 10, 6, and 5 Å for the γ phase.

The lattice thermal conductivity (κ_L) was computed by solving the Boltzmann transport equation as implemented in the ShengBTE software[47, 48]. A \mathbf{q} -mesh of $9 \times 9 \times 9$, $15 \times 15 \times 15$, and $21 \times 21 \times 21$ was adopted in the first irreducible Brillouin zone for the α , β , and γ phases, respectively, and with a Gaussian smearing width of 0.1. For the four-phonon (4ph) scattering rates were efficiently calculated by using the maximum likelihood estimation method with a sample size of 3×10^5 [49]. Furthermore, the influence of electron-phonon (el-ph) scattering for the β and γ phases was evaluated using the EPW code[50], along with QUANTUM ESPRESSO package[51]. In this work, the fully relativistic norm-conserving pseudopotentials that include the spin-orbit coupling (SOC) are employed[52]. A plane-wave energy cutoff of 100 Ry was adopted. For the Brillouin zone of MgAgSb, initial coarse grids of $8 \times 8 \times 8$ for k - and $4 \times 4 \times 4$ for q -points were used. These were subsequently interpolated onto dense $50 \times 50 \times 50$ grids via maximally localized Wannier functions. The κ_{ph} was computed using the ShengBTE package[24, 47, 53, 54], which was modified to incorporate both el-ph and 4ph scattering processes.

III.RESULTS AND DISCUSSION

Figures 1(a)-(c) illustrate the three primitive cell structures of MgAgSb within its operating temperature range. The low-temperature α phase (below $\sim 560\text{K}$)

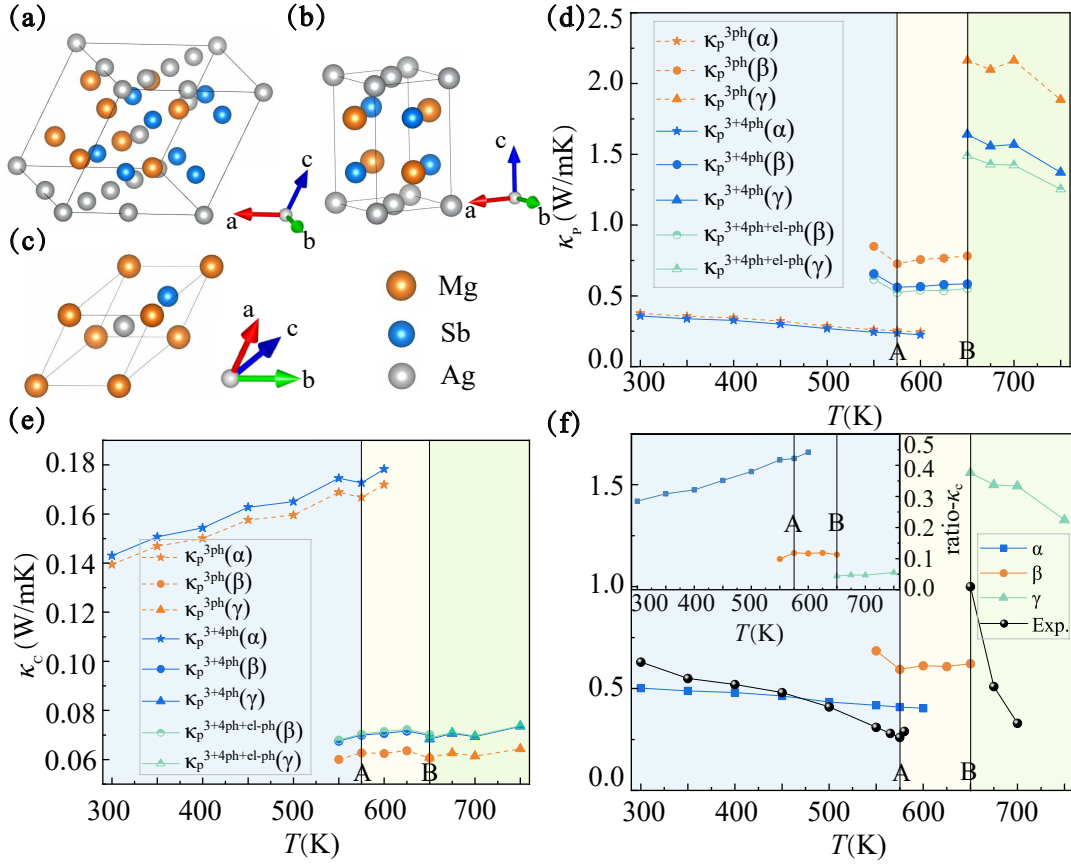


Figure 1. (a-c) The primitive cell of the α , the β , the γ phases of MgAgSb. The orange, blue, and silver colors represent Mg, Sb, and Ag atoms. The calculated (d) particle-like thermal conductivity (κ_p) and (e) the wave-like thermal conductivity (κ_c) for the three phases under 3ph, 3+4ph, 3+4ph+el-ph scattering. (f) Compares the calculated lattice thermal conductivity (κ_L) with experimental data, and the proportion of κ_c to κ_L . Phase transition point: A (575 K), B (650 K).

crystallizes in a tetragonal structure with space group $I-4c2$, containing 24 atoms—the most complex structure among the three phases. The intermediate β phase (~ 560 – 650 K) also adopts a tetragonal structure (space group $P4/nmm$) with 6 atoms. The high-temperature γ phase (above ~ 650 K) possesses a cubic structure (space group $F-43m$), consisting of only 3 atoms and having the highest symmetry[39].

Figure 1(d) presents the calculated particle-like thermal conductivity (κ_p) for the three phases under different scattering mechanisms. For the α phase, the inclusion of four-phonon (4ph) scattering has a negligible effect on κ_p , and its temperature dependence follows $\kappa_p \sim T^{-0.66}$. For the β phase, 4ph scattering reduces κ_p by 22.8% at 575 K compared to three-phonon (3ph) scattering alone, and additional electron-phonon (el-ph) scattering further reduces κ_p by 6.7%. Meanwhile, the β phase exhibits weak temperature dependence with a slight increase in κ_p between 575 and 650 K. For the γ phase, 4ph scattering reduces κ_p by 24.2% at 650 K compared to 3ph scattering alone, and el-ph scattering leads to an additional 9.2% reduction. Overall, κ_p follows the order $\alpha < \beta < \gamma$.

Figure 1(e) shows the wave-like thermal conductivity

(κ_c) as a function of temperature under different scattering mechanisms. κ_c generally increases with temperature for all phases. The α phase exhibits the most pronounced variation, rising from 0.14 W/mK at 300 K to 0.18 W/mK at 550 K—an increase of 28.6% at 3+4ph. In contrast, κ_c of the β and γ phases shows much weaker temperature dependence. For the β phase at 575 K, 4ph scattering increases κ_c by 11.5% compared to 3ph scattering alone, while el-ph scattering has a negligible effect. Similarly, for the γ phase at 650 K, 4ph scattering increases κ_c by 12.4% compared to 3ph scattering alone, with el-ph scattering again showing little impact.

Figure 1(f) compares the calculated lattice thermal conductivity (κ_L) with experimental data. For the α phase, the calculated κ_L (3,4ph) agrees well with experimental values[39]. Due to the weak temperature dependence of κ_p and the strong temperature dependence of κ_c , the overall κ_L exhibits a reduced temperature exponent, with $\kappa_L \sim T^{-0.33}$ [55]. For the β phase, $\kappa_L^{3+4ph+el-ph}$ shows a slight increase between 575 and 650 K, which arises from the intrinsic temperature dependence of the β phase. The experimental κ_L exhibits an upturn near 550–560 K, corresponding to the emergence of the β

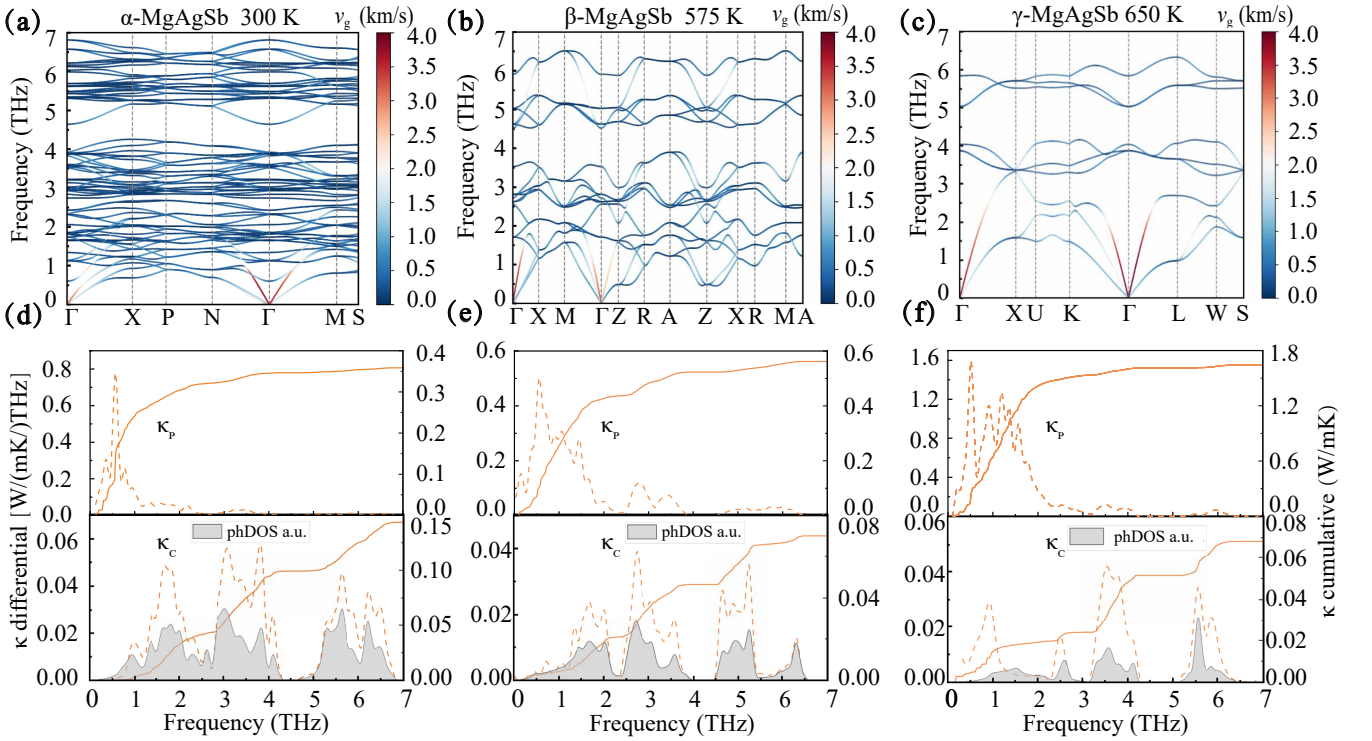


Figure 2. The phonon group velocity (v_g) projected onto the phonon dispersions of (a) α , (b) β , and (c) γ at 300 K, 575 K, 650 K, respectively. The cumulative and differential κ_p and κ_c as a function of phonon frequency and the phonon density of states (phDOS) of (d) α , (e) β , and (f) γ at 300 K, 575 K, 650 K, respectively.

phase. For the γ phase, the calculated $\kappa_L^{3+4\text{ph}+\text{el-ph}}$ at 650 K is 1.56 W/mK, notably higher than the experimental value of 1 W/mK. The deviation may mainly stem from the presence of impurities in the experimental samples and the slow $\beta \rightarrow \gamma$ phase transition process which is in an unbalanced state. Moreover, the theoretical calculations are based on an ideal pure phase and do not fully consider the influence of the phase transition[39]. The inset in Figure 1(f) shows the proportion of κ_c to κ_L . Notably, in the α phase, κ_c contributes up to 44.3% of the total κ_L , consistent with the view that wave-like phonon transport plays a significant role in low- κ materials[56, 57].

To further analyze the values and differences of κ_L across the three phases, figure 2 presents an analysis of the phonon transmission characteristic, with all data calculated at each phase's respective temperature (α at 300 K, β at 575 K, and γ at 650 K). Figures 2(a)-(c) show the phonon group velocity (v_g) projected onto the phonon dispersions. The α phase exhibits the densest phonon spectrum and the softest acoustic branches, with a maximum acoustic frequency of 1.2 THz. Its acoustic v_g remains around 0.5 km/s over a broad frequency range (1-7 THz). The β phase shows a sparser spectrum, with acoustic branches extending to 1.9 THz and higher v_g values of about 1.0 km/s within the range of 2 to 7 THz. The γ phase, with only 3 atoms per cell, has the simplest spectrum, featuring acoustic branches up to 3.3 THz and v_g of 1.5 km/s above 3 THz. Figures 2(d)-(f) display

the cumulative and differential κ_p and κ_c as a function of phonon frequency for the three phases at their respective temperatures. For all phases, κ_p is predominantly contributed by low-frequency acoustic modes, where v_g is higher and dispersion is stronger. In contrast, κ_c is governed by phonon modes that contribute minimally to κ_p , primarily those located in high-phDOS regions. The differential of κ_c closely resembles the phonon density of states (phDOS) curve for all three phases. The flat and dense phonon spectrum of the α phase enables a large number of phonon pairs with small frequency differences ($\omega - \omega'$), thereby giving rise to its substantial κ_c . For the β and γ phases, the phonon spectra become sparse, the number of coherent phonons with a smaller frequency difference decreases[58]. Consequently, their κ_c values are much smaller than that of the α phase.

Figure 3 presents the phonon scattering rates as a function of frequency. For the α phase at 300 K (Figure 3a), 3ph scattering dominates across the entire frequency range, with rates substantially higher than those of 4ph scattering. At low frequencies near 1 THz, the 3ph scattering rate is 0.31 ps^{-1} , whereas the 4ph contribution remains as low as 0.01 ps^{-1} . This negligible 4ph scattering is consistent with the minimal reduction in κ_p observed when including 4ph processes in the α phase. In contrast, the β at 575 K (Figure 3b) and γ at 650 K (Figure 3c) phases exhibit more complex scattering characteristics. For the β phase, 3ph scattering remains the strongest

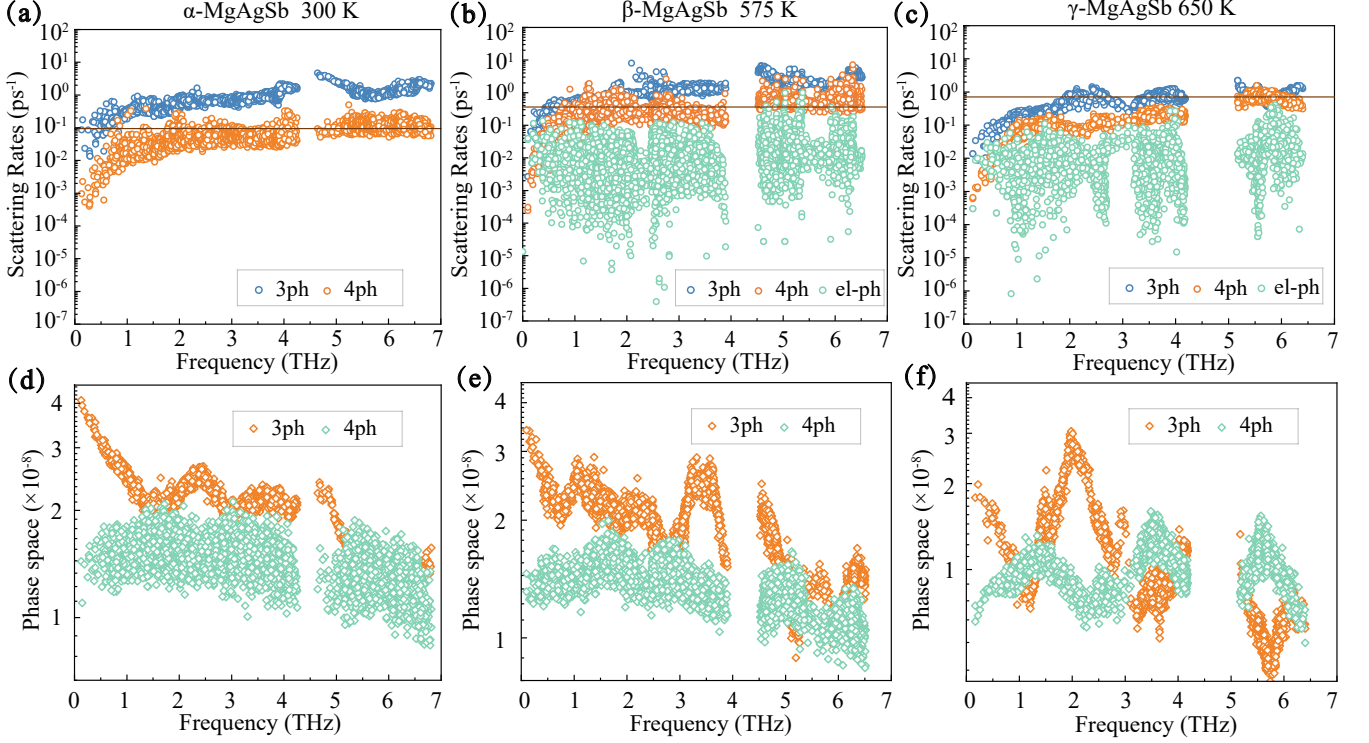


Figure 3. The phonon scattering rates of (a) α , (b) β , and (c) γ at 300 K, 575 K, 650 K, respectively. The three-phonon (P_3) and four-phonon (P_4) phase space for (d) α , (e) β , and (f) γ at 300 K, 575 K, 650 K, respectively.

overall, followed by 4ph and el-ph scattering. Notably, in the frequency range of 1–2.5 THz, the 4ph scattering rates become comparable to those of 3ph processes, both lying within the same order of magnitude. Additionally, at very low frequencies (0–1 THz), el-ph scattering has a significant effect on the partial phonon modes, with rates approaching those of 3ph and 4ph scattering. Similarly, for the γ phase, 3ph scattering generally dominates, yet 4ph scattering rates are comparable to 3ph in the 1–2 THz and 3–4 THz ranges. As in the β phase, el-ph scattering also becomes appreciable for low-frequency modes below 1 THz. The enhanced role of 4ph scattering in the β and γ phases correlates directly with the notable reduction in κ_p upon inclusion of 4ph processes. A horizontal dashed line in each panel marks the Wigner limit, defined as $\Delta\omega = \omega_{\max}/3n$, where ω_{\max} is the maximum phonon frequency and n is the number of atoms per primitive cell. Phonon modes above this line are considered to contribute predominantly to the κ_c [59]. Compared to the α phase, the β and γ phases exhibit substantially fewer phonon modes above the Wigner limit, which is consistent with their lower κ_c values, and further supports the explanation that in the more symmetric phase state, coherent phonon transmission is significantly suppressed.

To clarify how scattering rates influence κ_L across different phases, Figure S1 compares the phonon scattering rates between different phases at the same temperature. All the three phases take into account all the scattering situations. At 575 K, the scattering rates of the α and β

phases are close (Figure S1a). Given that the total heat capacity (c_v) of the β phase is only 0.9% higher than that of the α phase, the lower κ_L of the α phase can be primarily attributed to its reduced acoustic branch c_v and lower v_g . At 650 K, the scattering rate of the β phase is higher than that of the γ phase (Figure S1b). For instance, near 1.1 THz, the scattering rate of the β phase is $\sim 0.89 \text{ ps}^{-1}$, compared to only 0.21 ps^{-1} for the γ phase. Additionally, the total c_v of the β phase is 4% higher than that of the γ phase. However, the β phase larger unit cell size reduces the contribution of the acoustic branch, and the acoustic branch plays a dominant role in heat transfer. Therefore, phonon scattering is the main factor determining the difference in κ_L between the β and γ phases.

The three-phonon (P_3) and four-phonon (P_4) phase space for the α phase at 300 K, the β phase at 575 K, and the γ phase at 650 K are presented in Figures 3(d)–(f). The larger phase space typically implies the existence of more available scattering channels, which simultaneously satisfy the conditions of energy and momentum conservation[60]. The α phase has a dense and flat phonon spectrum, which is conducive to satisfying the conservation conditions and makes it have the largest P_3 among the three phases. As the number of primitive cell atoms decreases from the α phase to the β phase and then to the γ phase, the phonon spectrum becomes sparse, resulting in a significant decrease in P_3 . Meanwhile, P_4 also decreases with the simplification of the structure, but the decrease is smaller. Therefore, in the

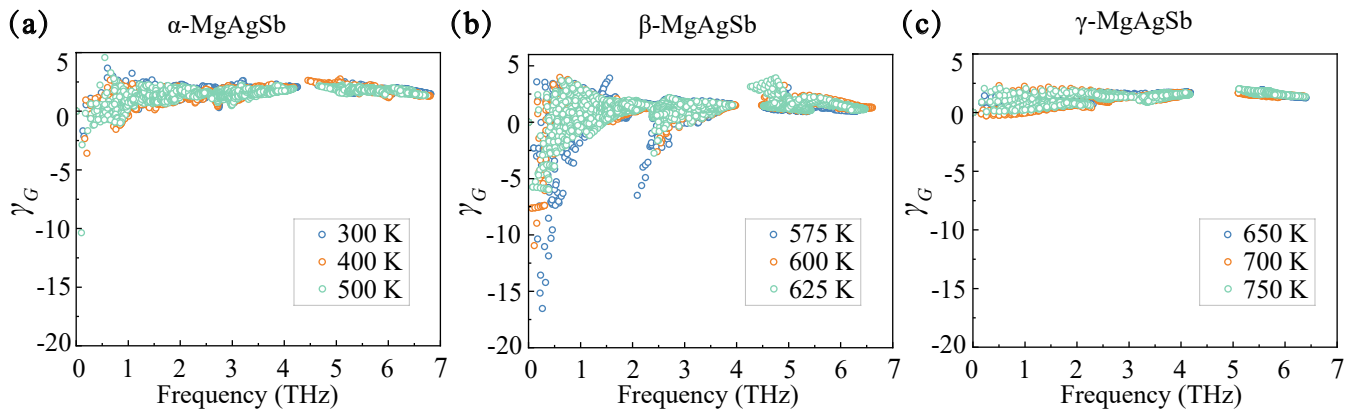


Figure 4. The Grüneisen parameters (γ_G) of (a) α -MgAgSb, (b) β -MgAgSb, and (c) γ -MgAgSb, at their respective temperatures.

γ phase, the contribution of P_4 becomes more significant.

Figure 4 shows the Grüneisen parameters (γ_G) of the three MgAgSb phases at their respective temperatures, which reflect the anharmonic characteristics. Here, the degree of anharmonicity is evaluated by the absolute value of γ_G . In the α and γ phases (Figures 4a and 4c), $|\gamma_G|$ does not change significantly within their respective temperature ranges. In contrast, for the β phase (Figure 4b), the $|\gamma_G|$ decreases markedly with rising temperature, indicating a gradual weakening of lattice anharmonicity. This reduces the temperature dependence of κ_p and leads to a slight increase in κ_p between 575 and 650 K.

IV. CONCLUSIONS

In summary, we have systematically investigated the lattice thermal transport across the α , β , and γ phases of MgAgSb using first-principles calculations. Our results reveal a progressive increase in κ_L following $\alpha < \beta < \gamma$, originating from distinct phase-dependent scattering characteristics. The 4ph scattering plays a crucial role in suppressing κ_p in the β and γ phases, reducing it by 22.8% at 575 K and 24.2% at 650 K, respectively.

While el-ph scattering provides additional reduction of 6.7% and 9.2%, respectively. The κ_c is most significant in the structurally complex α phase, accounting for up to 44% of the κ_L , and exhibits a pronounced increase with temperature. Meanwhile, the temperature dependence of κ_p is weak, leading to a weak overall temperature dependence ($\kappa_L \sim T^{-0.33}$) of the α phase. The weak temperature dependence of the β phase is attributed to a decreasing γ_G with rising temperature. These findings establish a comprehensive microscopic picture of phase-dependent thermal transport in MgAgSb.

IV. ACKNOWLEDGEMENTS

This work is supported by the Natural Science Foundation of China (Grants No. 12304038, 52206092, 12204402), the National Key Research and Development Program of China (Grants No. 2024YFA1409800), the Big Data Computing Center of Southeast University and the Center for Fundamental and Interdisciplinary Sciences of Southeast University, Basic Research Program of Jiangsu (BK20250035), Major Basic Research Project of the Natural Science Foundation of the Jiangsu Higher Education Institutions (25KJA470006).

-
- [1] G. Wang, Z. Tang, Y. Gao, P. Liu, Y. Li, A. Li, and X. Chen, Phase change thermal storage materials for interdisciplinary applications, *Chem. Rev.* **123**, 6953 (2023).
- [2] B. Jiang, P. Qiu, H. Chen, J. Huang, T. Mao, Y. Wang, Q. Song, D. Ren, X. Shi, and L. Chen, Entropy optimized phase transitions and improved thermoelectric performance in n-type liquid-like Ag_9GaSe_6 materials, *Mater. Today Phys.* **5**, 20 (2018).
- [3] Y. Yu and M. Wuttig, From phase-change materials to thermoelectrics: The role of metavalent bonding, *J. Mater. Res.* **40**, 1747 (2025).
- [4] X.-L. Shi, J. Zou, and Z.-G. Chen, Advanced thermoelectric design: From materials and structures to devices, *Chem. Rev.* **120**, 7399 (2020).
- [5] F. Chebli and F. Mechighel, Phase change materials: classification, use, phase transitions, and heat transfer enhancement techniques: a comprehensive review, *J. Therm. Anal. Calorim.* **150**, 1353 (2025).
- [6] M. Omini and A. Sparavigna, An iterative approach to the phonon boltzmann equation in the theory of thermal conductivity, *Physica B.* **212**, 101 (1995).
- [7] X. Yang, Z. Dai, Y. Zhao, J. Liu, and S. Meng, Low lattice thermal conductivity and excellent thermoelectric behavior in Li_3Sb and Li_3Bi , *J. Phys.:Condens. Mat.* **30**, 425401 (2018).
- [8] Z. Li, H. Xie, S. Hao, Y. Xia, X. Su, M. G. Kanatzidis, C. Wolverton, and X. Tang, Optical phonon dominated

- heat transport: A first-principles thermal conductivity study of BaSnS₂, *Phys. Rev. B* **104**, 245209 (2021).
- [9] M. N. Luckyanova, J. Garg, K. Esfarjani, A. Jandl, M. T. Bulsara, A. J. Schmidt, A. J. Minnich, S. Chen, M. S. Dresselhaus, Z. Ren, E. A. Fitzgerald, and G. Chen, Coherent phonon heat conduction in superlattices, *Science* **338**, 936 (2012).
- [10] J. Wang, Y. Hashimoto, J. Kono, A. Oiwa, H. Munekata, G. D. Sanders, and C. J. Stanton, Propagating coherent acoustic phonon wave packets in In_xMn_{1-x}As/GaSb, *Phys. Rev. B* **72**, 153311 (2005).
- [11] C. Colvard, R. Merlin, M. V. Klein, and A. C. Gossard, Observation of folded acoustic phonons in a semiconductor superlattice, *Phys. Rev. Lett.* **45**, 298 (1980).
- [12] X. Zeng, G. Niu, X. Wang, J. Jiang, L. Sui, Y. Zhang, A. Chen, M. Jin, and K. Yuan, Strain-engineered thermoelectric performance in superatomic semiconductor Re₆Se₈Cl₂: The role of four-phonon scattering and coherent phonons, *J. Phys. Chem. Lett.* **16**, 3122 (2025).
- [13] M. Simoncelli, N. Marzari, and F. Mauri, Wigner formulation of thermal transport in solids, *Phys. Rev. X* **12**, 041011 (2022).
- [14] L. Legenstein, L. Reicht, S. Wieser, M. Simoncelli, and E. Zojer, Heat transport in crystalline organic semiconductors: coexistence of phonon propagation and tunneling, *npj Comput. Mater.* **11**, 29 (2025).
- [15] L. Isaeva, G. Barbalinardo, D. Donadio, and S. Baroni, Modeling heat transport in crystals and glasses from a unified lattice-dynamical approach, *Nat. Commu.* **10**, 3853 (2019).
- [16] S. Mukhopadhyay, D. S. Parker, B. C. Sales, A. A. Puretzky, M. A. McGuire, and L. Lindsay, Two-channel model for ultralow thermal conductivity of crystalline Tl₃VSe₄, *Science* **360**, 1455 (2018).
- [17] S. Shenogin, A. Bodapati, P. Keblinski, and A. J. H. McGaughey, Predicting the thermal conductivity of inorganic and polymeric glasses: The role of anharmonicity, *J. Appl. Phys.* **105**, 034906 (2009).
- [18] Z. Zhang, Y. Guo, M. Bescond, J. Chen, M. Nomura, and S. Volz, Generalized decay law for particlelike and wave-like thermal phonons, *Phys. Rev. B* **103**, 184307 (2021).
- [19] A. Das and P. Banerji, Antibonding or nonbonding interaction-driven phonon modes softening and wave-like interband thermal conduction in layered In₄Te₃ under the framework of wigner transport formalism, *ACS Appl. Energy Mater.* **6**, 11521 (2023).
- [20] X. Yang, T. Feng, J. Li, and X. Ruan, Stronger role of four-phonon scattering than three-phonon scattering in thermal conductivity of III-V semiconductors at room temperature, *Phys. Rev. B* **100**, 245203 (2019).
- [21] Y. Xia, V. I. Hegde, K. Pal, X. Hua, D. Gaines, S. Patel, J. He, M. Aykol, and C. Wolverton, High-throughput study of lattice thermal conductivity in binary rocksalt and zinc blende compounds including higher-order anharmonicity, *Phys. Rev. X* **10**, 041029 (2020).
- [22] T. Feng and X. Ruan, Erratum: Quantum mechanical prediction of four-phonon scattering rates and reduced thermal conductivity of solids, *Phys. Rev. B* **97**, 079901 (2018).
- [23] N. K. Ravichandran and D. Broido, Phonon-phonon interactions in strongly bonded solids: Selection rules and higher-order processes, *Phys. Rev. X* **10**, 021063 (2020).
- [24] L. Ji, A. Huang, Y. Huo, Y.-m. Ding, S. Zeng, Y. Wu, and L. Zhou, Influence of four-phonon scattering and wave-like phonon tunneling effects on the thermal transport properties of TlBiSe₂, *Phys. Rev. B* **109**, 214307 (2024).
- [25] T. Tadano and S. Tsuneyuki, Self-consistent phonon calculations of lattice dynamical properties in cubic SrTiO₃ with first-principles anharmonic force constants, *Phys. Rev. B* **92**, 054301 (2015).
- [26] M. Simoncelli, N. Marzari, and F. Mauri, Unified theory of thermal transport in crystals and glasses, *Nat. Phys.* **15**, 809 (2019).
- [27] X. Wang, Z. Gao, G. Zhu, J. Ren, L. Hu, J. Sun, X. Ding, Y. Xia, and B. Li, Role of high-order anharmonicity and off-diagonal terms in thermal conductivity: A case study of multiphase CsPbBr₃, *Phys. Rev. B* **107**, 214308 (2023).
- [28] B. Liao, B. Qiu, J. Zhou, S. Huberman, K. Esfarjani, and G. Chen, Significant reduction of lattice thermal conductivity by the electron-phonon interaction in silicon with high carrier concentrations: A first-principles study, *Phys. Rev. Lett.* **114**, 115901 (2015).
- [29] A. Jain and A. J. H. McGaughey, Thermal transport by phonons and electrons in aluminum, silver, and gold from first principles, *Phys. Rev. B* **93**, 081206 (2016).
- [30] Y. Wang, Z. Lu, and X. Ruan, First principles calculation of lattice thermal conductivity of metals considering phonon-phonon and phonon-electron scattering, *J. Appl. Phys.* **119**, 225109 (2016).
- [31] J. Yang, D. T. Morelli, G. P. Meisner, W. Chen, J. S. Dyck, and C. Uher, Influence of electron-phonon interaction on the lattice thermal conductivity of Co_{1-x}Ni_xSb₃, *Phys. Rev. B* **65**, 094115 (2002).
- [32] A. Kundu, X. Yang, J. Ma, T. Feng, J. Carrete, X. Ruan, G. K. Madsen, and W. Li, Ultrahigh thermal conductivity of θ -phase tantalum nitride, *Phys. Rev. Lett.* **126**, 115901 (2021).
- [33] S. D. Wijeyesekera and R. Hoffmann, Transition metal carbides. a comparison of bonding in extended and molecular interstitial carbides, *Organometallics* **3**, 949 (1984).
- [34] H. Zhao, J. Sui, Z. Tang, Y. Lan, Q. Jie, D. Kraemer, K. McEnaney, A. Guloy, G. Chen, and Z. Ren, High thermoelectric performance of MgAgSb-based materials, *Nano Energy* **7**, 97 (2014).
- [35] M. J. Kirkham, A. M. dos Santos, C. J. Rawn, E. Lara-Curzio, J. W. Sharp, and A. J. Thompson, *abinitio* determination of crystal structures of the thermoelectric material MgAgSb, *Phys. Rev. B* **85**, 144120 (2012).
- [36] A. Li, L. Wang, X. Wu, J. Li, X. Wang, G. Wu, Z. Hu, and T. Mori, Semiconductor-metal transition powers high-efficiency MgAgSb thermoelectrics, *Sci. Adv.* **11**, eadx7115 (2025).
- [37] L. Xie, L. Yin, Y. Yu, G. Peng, S. Song, P. Ying, S. Cai, Y. Sun, W. Shi, H. Wu, N. Qu, F. Guo, W. Cai, H. Wu, Q. Zhang, K. Nielsch, Z. Ren, Z. Liu, and J. Sui, Screening strategy for developing thermoelectric interface materials, *Science* **382**, 921 (2023).
- [38] Z. Liu, J. Mao, J. Sui, and Z. Ren, High thermoelectric performance of α -MgAgSb for power generation, *Energy Environ. Sci.* **11**, 23 (2018).
- [39] Y. Huang, J. Lei, H. Chen, Z. Zhou, H. Dong, S. Yang, H. Gao, T.-R. Wei, K. Zhao, and X. Shi, Intrinsically high thermoelectric performance in near-room-temperature α -MgAgSb materials, *Acta Mater.* **249**, 118847 (2023).
- [40] S. Y. Back, S. Meikle, and T. Mori, Comprehensive study of α -MgAgSb: Microstructure, carrier transport properties, and thermoelectric performance under ball milling

- techniques, *J. Mater. Sci. Technol.* **227**, 57 (2025).
- [41] P. Ying, X. Liu, C. Fu, X. Yue, H. Xie, X. Zhao, W. Zhang, and T. Zhu, High performance α -MgAgSb thermoelectric materials for low temperature power generation, *Chem. Mater.* **27**, 909 (2015).
- [42] J.-L. Mi, P.-J. Ying, M. Sist, H. Reardon, P. Zhang, T.-J. Zhu, X.-B. Zhao, and B. B. Iversen, Elaborating the crystal structures of MgAgSb thermoelectric compound: Polymorphs and atomic disorders, *Chem. Mater.* **29**, 6378 (2017).
- [43] G. Kresse and J. Furthmüller, Efficient iterative schemes for ab initio total-energy calculations using a plane-wave basis set, *Phys. Rev. B* **54**, 11169 (1996).
- [44] J. P. Perdew, A. Ruzsinszky, G. I. Csonka, O. A. Vydrov, G. E. Scuseria, L. A. Constantin, X. Zhou, and K. Burke, Restoring the density-gradient expansion for exchange in solids and surfaces, *Phys. Rev. Lett.* **100**, 136406 (2008).
- [45] O. Hellman and I. A. Abrikosov, Temperature-dependent effective third-order interatomic force constants from first principles, *Phys. Rev. B* **88**, 144301 (2013).
- [46] F. Knoop, N. Shulumba, A. Castellano, J. P. A. Batista, R. Farris, M. J. Verstraete, M. Heine, D. Broido, D. S. Kim, J. Klarbring, I. A. Abrikosov, S. I. Simak, and O. Hellman, Tdep: Temperature dependent effective potentials, *J. Open Source Softw.* **9**, 6150 (2024).
- [47] W. Li, J. Carrete, N. A. Katcho, and N. Mingo, Shengbte: A solver of the boltzmann transport equation for phonons, *Comput. Phys. Commu.* **185**, 1747 (2014).
- [48] Z. Han, X. Yang, W. Li, T. Feng, and X. Ruan, Four-phonon: An extension module to shengbte for computing four-phonon scattering rates and thermal conductivity, *Comput. Phys. Commun.* **270**, 108179 (2022).
- [49] Z. Guo, Z. Han, D. Feng, G. Lin, and X. Ruan, Sampling-accelerated prediction of phonon scattering rates for converged thermal conductivity and radiative properties, *npj Comput. Mater.* **10**, 31 (2024).
- [50] S. Ponc e, E. Margine, C. Verdi, and F. Giustino, EPW: Electron-phonon coupling, transport and superconducting properties using maximally localized wannier functions, *Comput. Phys. Commun.* **209**, 116 (2016).
- [51] P. Giannozzi, S. Baroni, N. Bonini, M. Calandra, R. Car, C. Cavazzoni, D. Ceresoli, G. L. Chiarotti, M. Cococcioni, I. Dabo, A. D. Corso, S. de Gironcoli, S. Fabris, G. Fratesi, R. Gebauer, U. Gerstmann, C. Gougoussis, A. Kokalj, M. Lazzeri, L. Martin-Samos, N. Marzari, F. Mauri, R. Mazzarello, S. Paolini, A. Pasquarello, L. Paulatto, C. Sbraccia, S. Scandolo, G. Sclauzero, A. P. Seitsonen, A. Smogunov, P. Umari, and R. M. Wentzcovitch, QUANTUM ESPRESSO: a modular and open-source software project for quantum simulations of materials, *J. Phys.:Condens. Matter* **21**, 395502 (2009).
- [52] D. R. Hamann, Optimized norm-conserving vanderbilt pseudopotentials, *Phys. Rev. B* **88**, 085117 (2013).
- [53] W. Li, N. Mingo, L. Lindsay, D. A. Broido, D. A. Stewart, and N. A. Katcho, Thermal conductivity of diamond nanowires from first principles, *Phys. Rev. B* **85**, 195436 (2012).
- [54] W. Li, L. Lindsay, D. A. Broido, D. A. Stewart, and N. Mingo, Thermal conductivity of bulk and nanowire Mg₂Si_xSn_{1-x} alloys from first principles, *Phys. Rev. B* **86**, 174307 (2012).
- [55] N. Ouyang, D. Shen, C. Wang, R. Cheng, Q. Wang, and Y. Chen, Positive temperature-dependent thermal conductivity induced by wavelike phonons in complex Ag-based argyrodites, *Phys. Rev. B* **111**, 064307 (2025).
- [56] Y.-M. Zhao, X. Zhang, C. Zhang, S. Shin, and L. Shen, Dual-channel phonon transport in two-dimensional materials with low thermal conductivity, *Phys. Rev. B* **112**, 125406 (2025).
- [57] J. Zheng, C. Lin, C. Lin, G. Hautier, R. Guo, and B. Huang, Unravelling ultralow thermal conductivity in perovskite Cs₂AgBiBr₆: dominant wave-like phonon tunnelling and strong anharmonicity, *npj Comput. Mater.* **10**, 30 (2024).
- [58] Y. Wu, Y. Chen, Z. Fang, Y. Ding, Q. Li, K. Xue, H. Shao, H. Zhang, and L. Zhou, Ultralow lattice thermal transport and considerable wave-like phonon tunneling in chalcogenide perovskite BaZrS₃, *J. Phys. Chem. Lett.* **14**, 11465 (2023).
- [59] E. Di Lucente, M. Simoncelli, and N. Marzari, Crossover from boltzmann to wigner thermal transport in thermoelectric skutterudites, *Phys. Rev. Res.* **5**, 033125 (2023).
- [60] Y. Li, J. Chen, C. Lu, H. Fukui, X. Yu, C. Li, J. Zhao, X. Wang, W. Wang, and J. Hong, Multiphonon interaction and thermal conductivity in half-Heusler LuNiBi, *Phys. Rev. B* **109**, 174302 (2024).